CI&CEQ
Chemical Industry & Chemical Engineering Quarterly

Available online at
Association of the Chemical Engineers of Serbia AChE
www.ache.org.rs/CICEQ

Chem. Ind. Chem. Eng. Q. 30 (4) 335–348 (2024) CI&CEQ

CHITRA DEVI VENKATACHALAM[1]
PREMKUMAR BHUVANESHWARAN[1]
MOTHIL SENGOTTIAN[2]
SATHISH RAAM RAVICHANDRAN[2]

[1]Department of Food Technology, Kongu Engineering College, Perundurai, Tamil Nadu, India.

[2]Department of Chemical Engineering, Kongu Engineering College, Perundurai, Tamil Nadu, India

RELIABILITY-BASED DESIGN OPTIMIZATION OF SCREW SHAFT FOR CONTINUOUS HIGH-PRESSURE HYDROTHERMAL CO-LIQUEFACTION PROCESS

Article Highlights

- Structural analysis was performed on the screw-shaft to withstand high pressure in HTCL reactor
- The uniformly varying pressure was applied to the screw shaft to calculate its structural strength
- Helix angle, depth, pitch, and flight length were the dimensional parameters optimized
- Stress, deformation, shear, and bending stress were crucial responses used for structural analysis
- GFRG, SN ratio, and ANOVA methods were used for optimization and recommended for structural simulations

Abstract

Hydrothermal co-liquefaction (HTCL) is the prominent process for producing bio-products with a higher conversion rate. It is performed at high temperatures and pressure in the presence of water. Earlier, it was mostly conducted in batch reactors, but it has major limitations including operating volume, back mixing, and tedious process for high productivity. With that, the present investigation is performed on designing the screw shaft for the high-pressure HTCL process. The dimensional factors including flight length, pitch, helix angle, and depth were considered to design the optimal screw shaft. Likewise, principal stresses, shear stress, bending stress, bending moment, and total deformation were regarded as inevitable response variables to analyze the internal strength of the shaft. In this regard, the Taguchi approach provides the L_9 (3^4) orthogonal array as an experimental design. Then, the numerical results from the transient structural analysis were analyzed with the assistance of statistical methods such as Grey Relational Grade (GRG), Grey Fuzzy Reasoning Grade, Analysis of Variance (ANOVA), and Taguchi method to find the most influential dimensions for minimizing the response variable. Consequently, the results from both GRG and Taguchi optimization were compared, and selected the most optimum parameters.

Keywords: hydrothermal co-liquefaction, screw shaft, finite element method, stress analysis, Goodman failure criteria, multi and single response optimization technique.

SCIENTIFIC PAPER

UDC 5/6:620

As stated by the Energy Information Administration (EIA), the utilization of liquid fuels was 102.22 million barrels per day at the end of 2022 and also it is expected to increase by 2.4 % in forthcoming years.

These gradual increments in the utilization of conventional fuel and its future demand indirectly suggest the need for alternate fuels like biomass energy, which can be produced via thermochemical conversion processes [1]. The commercialization of these biomass conversion technologies would

Correspondence: C.D. Venkatachalam, Department of Food Technology, Kongu Engineering College, Perundurai, Tamil Nadu - 638060, India.
E-mail: erchitrasuresh@gmail.com
Paper received: 24 November, 2023
Paper revised: 14 February, 2024
Paper accepted: 24 February, 2024

https://doi.org/10.2298/CICEQ231124004V

decrease the emission of greenhouse gases and pollutant particulates, thereby reducing global warming [2]. Among different thermochemical conversion processes, hydrothermal co-liquefaction (HTCL) is the most promising process for the quick conversion of biomass into bio-liquid under both sub-critical and supercritical conditions because of using water as solvent and catalyst. HTCL process focuses on the biological degradation of feedstock at higher temperatures (250 °C to 350 °C) and pressure (20 MPa to 25 MPa) to produce a high amount of bio-crude rather than biosolid and biogas [3,4].

In the last few decades, the HTCL process was performed in single and sequence-type hydrothermal batch reactors for various types of biomass conversion. The capacity of these reactors was in the range of 5 mL to 800 mL, and it also consisted of agitators and electrical band heaters to improve the heat transfer and enhance mixing during the hydrothermal conversion. Some of the major limitations of batch reactors including back mixing and inconsistency of the bioproducts are eliminated in the current HTCL reactor [5–7]. Additionally, a wide range of particle sizes can be used in this reactor compared to batch reactors. In the batch reactor, biomass heating, cooling, discharging, and refilling were time-consuming processes that led to lower energy efficiency. Some researchers have also carried out the same process in a semi-continuous reactor using a high-pressure piston feeder with a heat exchanger in the closed chamber. The major drawback of this process is the use of higher input energy for the high-pressure piston pump of 30 MPa as it also increases the operating cost. [8,9].

To overcome these limitations, Efika *et al.* (2012) and Shengbo *et al.* (2021) performed thermochemical reactions on screw-type reactors for quick transportation and biomass conversion. A two-stage screw kiln reactor (screw diameter = 6 cm and length = 54 cm) was used for the production of syngas from the waste biomass through pyrolysis which is operated at temperatures between 500 °C and 760 °C and it resulted in better biomass mixing and better heat transfer rate than batch reactors [10,11]. Likewise, Hoekman *et al.* (2017) developed a twin-screw extruder (having a 25 mm diameter) operating at high pressure of 25 MPa and temperature of 350 °C. It exhibited a shorter residence time (21–28 sec) compared to the conventional reactor [12]. In addition, an auger-type screw reactor was used for recycling the plastic waste through pyrolysis, it is performed at temperatures between 380 °C and 600 °C with better axial dispersion and uniform flow in thermal conditions over the length with respect to time [13].

From the above studies, it was observed that these continuous-type screw reactors had quick processing rates, higher productivity, and less energy intake. Moreover, the efficiency and chemical properties of the biofuel were also found to be improved in the screw-type continuous reactor with shorter residence time regardless of the thermochemical process [2,10,11,14,15]. Especially, the auger screw was preferred for pyrolysis due to the transition of dry grains and in the case of wet feedstock, the Archimedes screw was preferred for the better transition of particles in the form of slurry [16,17].

Finite Element Method (FEM) is a widely used technique to model and theoretically evaluate the structural integrity of any mechanical component. Likewise, Goodman criteria are preferred while performing the failure analysis under dynamic conditions and it has been used in various designs of components such as the main shaft in gas turbine engines, drive shaft, turbine shaft, and propeller shaft [18,19]. Further, the Grey Relational Grade (GRG) is the most employed optimization technique for multiple responses where the direct responses were converted single response called Grey Relational Grade (GRG), and it is verified with the guidance of Grey Fuzzy Reasoning Grade (GFRG). Recently, it has been performed to achieve machining effectiveness [20], improving the tensile strength of the aluminum alloy pipe [21,22], enhancing the bending and torsional stiffness of the external structure of automobile [23], improving the static and dynamic performance of the drive shaft [18] and beam structure [24].

In the present study, the reactor under consideration consists of an Archimedes screw shaft rotated inside a cylindrical chamber employed with external band heaters, inside which the transition and chemical reaction of the feedstock takes place within the chamber. The shaft was designed to experience both torsional loads (due to shaft rotation) and bending loads (due to reaction pressure) during the continuous HTCL process. The screw shaft is the important component that pushes forward the feedstock towards the length of the reactor and it has to withstand high temperatures of 400 °C and pressure varying from 1 to 25 MPa. To analyze the structural stability of the screw shaft and to study its resistance to stress and deformation at high-pressure FEM is used. In this study, flight length, pitch, depth, and helix angle were considered the vital dimensions to be optimized with respect to principal stresses, bending stress, shear stress, and total deformation. Here, the dimensions for the optimization study were considered by following the standard shaft design procedure. The optimum dimensions of the screw shaft were selected by using the multi-response optimization technique (grey relational grade method), single-response optimization technique (Taguchi's method), and its contribution as

an effective factor is predicted using ANOVA. The method followed for dimensional optimization is given in the flowchart as shown in Fig. 1.

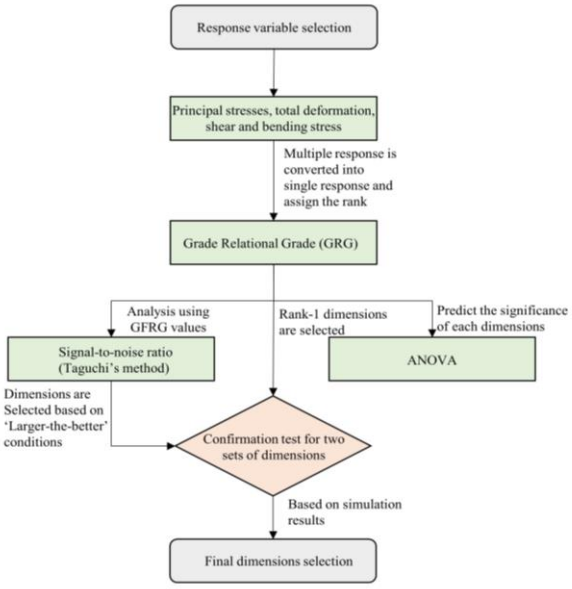

Figure 1. (a) Pressure contour plot; (b) pressure profile for screw shaft enclosed reaction chamber during high-pressure fluid flow.

MATERIALS AND METODS

Materials

During the HTCL process, the water which is used as the solvent becomes more acidic, and thus the screw shaft is more susceptible to corrosion. So, the screw shaft should be made of a material with easy machinability and high resistance to corrosion, wear, and chloride formation. Because of good acidic, corrosion, and chloride resistance, H13, SS304, and SS316 were initially considered to develop the screw shaft. However, SS304 and SS316 were not selected due to their inadequate mechanical properties such as yield and ultimate strength to sustain high stress, whereas H13 is selected for designing the screw shaft. The presence of high Chromium and molybdenum in H13 enhances the resistance to corrosion and chloride formation [25]. Table S1 (Supporting material) compares the mechanical properties like Young's modulus, bulk modulus, shear modulus, and tensile and compressive strength of H13 with SS304 and SS316, and these values were taken for Finite element analysis [26,27].

The screw shaft was modeled by using the Catia V5R21 for which the dimensions were obtained from the Design Expert Software version 8.0 as given in Table S2. The pressure distribution over the length of the screw shaft in each section of the reactor filled with biomass slurry was determined by fluent analysis. Furthermore, the Finite Element Method (FEM) was carried out for the discretization of the screw shaft where the structural analysis is performed to know the stress distribution, deformation, bending stress, and FOS through a transient structural module in Ansys R1.

Metodology

Specification of the screw shaft

Flight length, diameter, pitch, helix angle, and thread depth were considered the important dimensions to be optimized for designing an optimal shaft model. The size of depth is essential to find the cross-sectional area and is responsible for the shear and principal stress of the shaft. Likewise, flight length is the major factor responsible for the bendability of the shaft. At last, helix angle and pitch length were crucial parameters for the flowability of fluid in the shaft. Whence, the shaft diameter (58 mm) was fixed by applying the continuity equation (conservation of mass) given in Eq. (1) for the constant mass flow rate of biomass (1 kg/hr). In general, the L/D ratio ranging from 20 to 30 had chosen for the perfect extrusion of the feed material in the screw shaft and also the pitch was another salient parameter for transporting the biomass which ranges from 0.25 to 0.5 % of the screw diameter. In addition, the helix angle of the square thread provides better flow over the transportation which was calculated by using Eq. (2). The depth used for the square thread is always half of the screw pitch. Moreover, it was quite difficult to select the best value from each dimension to develop the optimized design of the screw shaft. Hence, the Design of Experiments (L_9 - Taguchi's model) was used to select the better combination of the dimensions to model the HTCL screw shaft as given in Table S2. The diameter of the reaction chamber was calculated through the Continuity equation given by:

The mass flow rate through the inlet $\dot{m}_1$ - mass flow rate through the outlet $\dot{m}_2$:

$$\dot{m}_1 = \rho A V \tag{1}$$

The equation for computing the helix angle of the screw shaft:

$$\phi = \tan^{-1}\left(\frac{P}{\pi D}\right) \tag{2}$$

where P - screw pitch, and D - screw diameter.

Finite Element Method (FEM) for the screw shaft

Fig. S1(a,b) illustrates the two-dimensional schematic diagram and 3-D model of the screw shaft used for the finite element analysis. The feed mixture enters zone "A" called as suction zone, and here the

feed material is freely moved along the screw shaft and it reaches the compression zones "B" and "C". The feedstock gets compressed and becomes finer particles during HTCL in this zone. A high-pressure water nozzle is provided to improve the chemical conversion and operating pressure in zone "D". Likewise, zones "E" and "G" represent the second and third compression zones, while "F" and "H" represent the expansion zones respectively. The high-pressure zones (C, D, E) are marked using a red box in Fig. S1 (a). Further, the discretization was made by converting the screw shaft into triangular elements using FEM during structural analysis. The governing Eqs. (3,4) were used for meshing the uniformly rotating shaft considering the gyroscopic effect and resisting moment. Further discretization of the screw shaft was done using the adaptive meshing technique for the size of 2 mm and is given in Fig. S1(c,d). Also, the high smoothing mesh was adapted to get better convergence results, especially on transient conditions [28–30]. For pure torsion acting on the screw shaft, it was assumed that the shaft material is homogeneous and perfectly elastic. It was also assumed that the torsional moment is uniform over the shaft length, the stress does not exceed the limit of proportionality and the deformation is negligible.

The global force equation for screw shaft using FEM is given by Eq. (3):

$$[K]\{u\} = \{F\} \tag{3}$$

where [K]- stiffness matrix, {u} - displacement matrix, and {F} - force matrix.

The derived FEM equation applied for meshing the screw shaft is given by Eq. (4):

$$\begin{Bmatrix} M_{x1} \\ M_{x2} \\ M_{y1} \\ M_{y2} \end{Bmatrix} = \frac{GL}{I} \begin{bmatrix} 1 & -1 & -1 & -1 \\ -1 & 1 & -1 & -1 \\ -1 & -1 & 1 & -1 \\ -1 & -1 & -1 & 1 \end{bmatrix} \begin{Bmatrix} \phi_{x1} \\ \phi_{x2} \\ \phi_{x3} \\ \phi_{x4} \end{Bmatrix} \tag{4}$$

Loading and boundary conditions

The uniformly varying pressure (from 1 MPa to 23 MPa) developed in different zones through the length of the HTCL reactor is given in Fig. S2(a). This pressure variation happens due to the alternate thread portion (left and right thread) in the screw shaft. It was observed that the screw shaft experienced a maximum torque of 125000 Nm while running at 60 rpm and a maximum pressure of 23 MPa. Fig. S2(a) shows the different pressure zones that were found by applying the HTCL operating conditions onto the screw shaft enclosed with the reaction chamber. The pressure analysis was performed using a fluent module pressure profile developed for similar HTCL conditions as shown in Fig. S2(b). It shows a gradual increment in pressure from 1 to 23 MPa till the length of 0.8 m, after which it starts to decrease significantly. High pressure was developed at the mid-section of the screw shaft due to the water injection. Likewise, a slight pressure decrease was observed at the end zones (F, G, H) of the screw shaft due to the choking of feedstock.

During the FEM analysis, the shaft was divided into seven zones based on the different pressure acting on each section of the screw shaft given in Fig. S1(a). In addition, the shaft is free to rotate and pressure (uniformly varying load) is acting in all directions. The analysis was carried out for 7 secs (number of steps) with a time step of 0.5 sec and solved using the work-energy method with governing equation as given in Eq. (4). It was considered that the pressure is acting gradually concerning time in each zone of the screw shaft under transient conditions and the time-dependent pressure was calculated by using the SN curve in FEM analysis shown in Table S3.

Response variable studies to optimize the design

Principal stresses, shear stress, bending moment, bending stress, total deformation, and Factor of Safety (FOS) were the crucial response variables considered for structural analysis. These variables were numerically estimated using the structural analysis in simulation software. Principal stresses were calculated to realize the internal strength of the screw shaft for the given dimensions. It should be less than the ultimate tensile strength (UTS) for any material and its cross-section to resist the external force. Maximum and minimum principal stresses were estimated by using Eq. (5) and it is acting on the corresponding planes, which the angle ranges from 0° to 180° in the finite element method [31,32]. Similarly, bending moment and deformation were considered to evaluate the amount of deflection and change of cross section during the action of external force. The bending moment might be varied along the overall length of the shaft, depending on the distribution of applied load [33]. It is necessary to ensure that the moment developed in the shaft should be within acceptable limits to avoid excessive deflection [34]. The bending moment was calculated by considering the shaft with a simply supported beam with a uniformly varying load which is given in Eq. (6). The Permanent deformation occurs when the stress value exceeds the yield stress and further increment of load leads to fracture due to shear and bending stress [35]. Bending and shear stress were the two major stresses responsible for estimating the fatigue failure or lifetime of the screw shaft. The maximum shear stress acting on the fractured surface of the screw shaft was estimated using Eq. (7).

The Goodman failure criteria given in Fig. 3 show the good relationship between bending and shear stress for calculating the endurance cycle and safe limits of the screw shaft [36].

Maximum and minimum principal stresses were calculated using σ_1 and σ_2 given by Eq. (5):

$$\sigma_{max,min} = \frac{\sigma_1+\sigma_2}{2} \pm \left[\frac{\sigma_1-\sigma_2}{2}\right] X\cos(2\theta) \quad (5)$$

The bending moment of the shaft with a simply supported beam with a uniformly varying load was calculated by using Eq. (6):

$$Bending\ moment, M = \left(\frac{WXL}{2}\right) - \left(\frac{WL^2}{2}\right) \quad (6)$$

The shear stress of any shaft was calculated by using Eq. (7):

$$\tau_{max} = \frac{TD}{2J} \quad (7)$$

Goodman's safety factor for the given dimensions of the screw shaft was estimated using Eq. (8) [36]:

$$\frac{\sigma_{ta}}{s_e} + \frac{\sigma_{tm}}{s_u} = \frac{1}{n} \quad (8)$$

where n - Goodman safe limit.

Total deformation of the screw shaft was calculated by using Eq. (9):

$$\sigma_{total} = \sqrt{X^2+Y^2+Z^2} \quad (9)$$

Procedure for dimensional optimization

The well-established procedure was followed to perform the dimensional optimization based on the flow chart given in Fig. 1. Firstly, the multiple responses were converted into a single response termed GFRG using the fuzzy method. Then, the GFRG result was applied to the signal-to-noise ratio method in Taguchi's technique to carry out single response optimization based on estimated variance. ANOVA was performed to realize the contribution of individual dimensions with respect to the response variable. The two sets of dimensions were predicted from Fuzzy and Taguchi's method. The screw shaft was designed depending on the predicted two sets of dimensions and the best simulation result was taken to the design and fabrication process.

Grade relational grade optimization method

The robustness of the dimensional factors for designing the screw shaft can be improved using a multi-response optimization method termed Grey Relational Grade (GRG). Initially, the normalized value is estimated from the primary results using Eqs. (10,11) based on the requirements of "Larger-the-better" or "Smaller-the-better" conditions. Then, the Grey Relational Coefficient (GRC) was calculated through Eq. (12) and it is an essential term to obtain the GRG values. The final results were verified with the Grey Fuzzy Reasoning Grade (GFRG) and evaluated by following the fuzzy logic. Fuzzification, Rule base, Decision making, and Defuzzification were the four major steps to be followed to bring the value of GFRG. In fuzzification, the Mamdani interface system was applied to relate the input and output parameters. Furthermore, the membership function was prepared using linguistic variables based on the sequential values of both input factors and output response (GRG value), which helps to generate the fuzzy rules. The rank was provided to both GRG and GFRG values depending on the highest value was graded as one and so on [20,37,38]. The normalized values of the original response sequence were obtained by:

$$y_n^* = \frac{y_n(q) - \min y_n(q)}{\max y_n(q) - \min y_n(q)} \quad (10)$$

if Larger-the-better.

$$y_n^* = \frac{\max y_n(q) - y_n(q)}{\max y_n(q) - \min y_n(q)} \quad (11)$$

if Smaller-the-better. Where, y_n^* - normalized value of respective runs, $y_n(q)$ - primary response value of respective run from simulation results, *max* $y_n(q)$ - maximum value of individual response variable, *min* $y_n(q)$ - minimum value of individual response variable, y_d^* - deviation of individual response from normalized value.

The grey relational coefficient (GRC) can be evaluated as follows:

$$\rho(q) = \frac{\Delta\min + \rho\Delta\max}{\Delta y_d^* + \rho\Delta\max} \quad (12)$$

where, $\rho(q)$ - Grey relational coefficient, $y_d^* = 1 - y_n^*$ - deviation from the normalized value, ρ - weightage for coefficient. Generally, ρ =0.5 was taken.

Taguchi's optimization technique

Taguchi's method plays a vital role in optimizing the dimensional parameters with respect to a single response at a minimal number of trials. It also uses the orthogonal array technique to build the design of experiments, which mainly depends on degrees of freedom. Taguchi produces the results based on calculating the mean and deviation of the response

variable. When the deviation is less or equal mean obtained, the response variable will not change concerning dimensional factors. In addition, the signal-to-noise analysis was also considered for building a sustainable model with minimum deviation [21,39,40]. In this regard, three levels with four factors (3^4) models were chosen for designing the efficient screw shaft. For 3^4 models, there were four orthogonal arrays (L_9, L_{12}, L_{16}, and L_{18}) available for constructing the design of experiments.

The GFRG attained from the Fuzzy Interface System (FIS) was implemented in Taguchi's method to find out the optimal values of dimensional factors. Here, the rank was provided to each parameter based on the deviation of the response variable. It was also expressed from the SN ratio graph by measuring the deviation from the target value relative to the noise present in the system. SN ratio is commonly classified into three types namely smaller-the-better, larger-the-better, and nominal-the-better based on the specific objective of the response variable which is given in Eqs. (13–15). Most of the stress values prefer the smaller-the-better type SN ratios to find the optimal dimensional factor [41,42].

When the response variable is recommended to be smaller then:

$$\alpha = -10\log\frac{1}{m}\sum_{a=1}^{m} z_i^2 \tag{13}$$

When the response variable is recommended to be nominal then:

$$\alpha = -10\log\frac{1}{m}\sum_{a=1}^{m} \frac{\mu^2}{\sigma^2} \tag{14}$$

When the response variable is recommended to be larger then:

$$\alpha = -10\log\frac{1}{m}\sum_{a=1}^{m} \frac{1}{z_i^2} \tag{15}$$

Analysis of Variance (ANOVA)

The statistical method (ANOVA) is applied to know the impact of the different factors with respect to the response variable. ANOVA uses the results that were obtained from the GRG optimization. It also defines the null and the alternative hypothesis to find the significance of the different factors by evaluating the means of the response variable. The *P* and *F* values are more important in choosing the suitable hypothesis based on significant values. In case, the *P*-value is less than or equal to 0.05, then the null hypothesis is not applicable for the particular response or else the specific factor is acceptable for the null hypothesis and also it shows a similar mean value at each level. Finally, *R*-squared and adjusted *R*-squared are the salient parameters for explaining the proportion of the variation of the response variable, which ranges from 0 to 1. Null hypothesis (H_o) means a similar response at each level of dimensional factors and alternative hypothesis (H_1) has a different response at each level of dimensional factors [21,40].

RESULTS AND DISCUSSION

Maximum and minimum principal stress affecting the screw shaft

Fig. 2a illustrates the maximum principal stress of the screw shaft, in which run-8 experience the low-stress value of 8.5176 x 10^7 Pa and run-2 exhibits the high stress of 5.9686 x 10^8 Pa was calculated using Eq. (5). Likewise, run-1, 4, 5 and 9 possess the stress values from 3 x 10^8 Pa to 3.7623 x 10^8 Pa and run-3, 6 and 7 resist the external force ranges from 1.05 x 10^8 Pa to 1.51 x 10^8 Pa. These stress values of the screw shaft are under the limit of bulk modulus (160 x 10^9 Pa) of H13. In the case of minimum principal stress given in Fig. 2b, the highest (1.7854 x 10^8 Pa) and lowest (2.2018 x 10^7 Pa) stress value was possessed by run-2 and run-8 respectively. The stress value ranges from 2.7148 x 10^7 Pa to 1.0834 x 10^8 Pa for the remaining sets of Taguchi's runs. By considering the above-mentioned principal stress value, the dimensions used for run-8 were suggested for designing the screw shaft due to their high resistance to external pressure.

Apart from principal stress, the stress ratio is also important for describing the fatigue life of the screw shaft. It is the ratio of the difference between minimum and maximum principal stress to the sum of these two stresses. Fatigue life mainly depends on the temperature, loading, and stress developed in the testing material. In addition, the stress ratio shows an indirect proportionality with the fatigue life [36,43]. In this regard, run-6 and run-2 have the lowest and highest stress ratios of 0.28 and 0.56 respectively. The stress ratio from 0.43 to 0.54 was possessed by the residual runs of the FEM analysis. From the aforementioned data, the dimensions suggested for run-6 and run-8 have higher fatigue life compared to other runs for the given loading conditions shown in Table S3. So, it withstands a large number of cycles under dynamic conditions of the screw shaft. It is also noted that the small L/D ratio delivers the higher fatigue life of the shaft and resists the maximum principal stress.

Total shear force and maximum bending moment acting on the screw shaft

The different dimensions of the screw shaft in

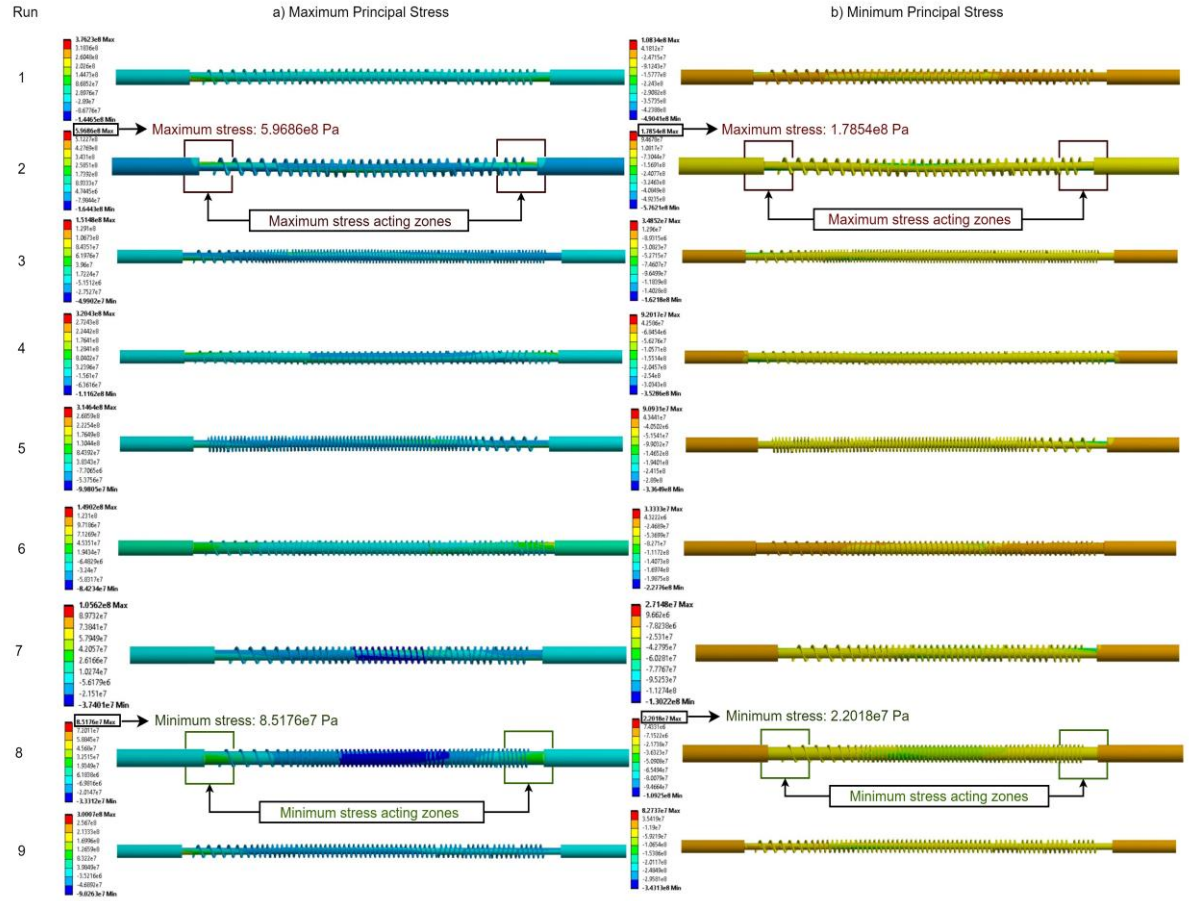

Figure 2. Contour plot for (a) maximum principal stress in Pa; (b) minimum principal stress in Pa under external pressure for Taguchi's design of screw shaft.

each run given in Table S2 were converted into the beam with a corresponding circular cross-section for beam analysis under the finite element method. The cross-section of each beam provides the different area moment of inertia in the Y and Z axes calculated using Eq. (6). Area moment of inertia always shows the indirect proportionality with the bending moment, which implies that the shaft will bend very less for a larger area moment of inertia. Moreover, it depends on the geometrical property of the shaft. The boundary conditions used for the beam analysis are similar to the stress analysis. The beam was segmented into seven sections based on the pressure acting on the shaft given in Fig. S1 (Supplementary material) and Fig.1a.

Shear force at the given section is the rate of change of bending moment with respect to the axial distance given in Eq. (7). It is also the first derivative and shows direct proportionality with the bending moment. In this regard, the bending moment should be minimal for any cross section to withstand the deflection. Additionally, the bending moment mainly depends on the nature and magnitude of the load, type of support, and also dimensional parameters like flight length, diameter, and depth of the shaft [34,44]. Now, the type of load and support are similar for each model of the screw shaft. In this respect, Fig. S3b shows the lowest (9537.2 Nm) and highest (14884 Nm) bending moments of the screw shaft exhibited by run-2 and run-4 respectively. The bending moment lies between 9646.8 Nm and 14771 Nm for the rest of Taguchi's runs. There was a slight difference in bending moment (110 Nm) between run-2 and run-8. As recommended in the principal stress, the dimensions applied for run-2 and run-8 are suitable for designing the screw shaft with minimum bending effects due to having less area moment of inertia compared to the remaining models. Also, these runs have a smaller L/D ratio to resist the bending against the external load.

Influence of maximum bending and shear stress on the screw shaft

Figs. S4a and S4b illustrate the contour plot for bending and shear stress, which were derived by solving the FEM equation under transient conditions. These stresses mainly depend on the geometrical dimensions like radius (distance from the neutral axis), length, and helix angle of the shaft and it should be minimum for any material to withstand the fatigue

failure. In the present study, the minimum values of bending (9.1276 x 10^8 Pa) and shear stress (3.7969 x 10^7 Pa) were experienced in run-8, which also exhibits the maximum fatigue safety factor of n=1.2 estimated using Eq. (8). Moreover, run-8 withstands the stress of 1.2 times higher than the allowable stress of H13. Table S4 shows the maximum endurance limit of 10^7 was observed for run-8, as a result of the intersection of bending and shear stress acting below the modified Goodman line shown in Fig. 3. Meanwhile, run-9 shows the maximum bending stress value of 4.9549 x 10^9 Pa and its corresponding shear stress of 1.2643 x 10^8 Pa but it possesses the minimum safety factor of 0.21 and endurance limit of 10^3, which was inappropriate dimensions for designing the screw shaft. It was noticed that the wide range of bending and shear stress was perceived for the remaining runs from 1.2169 x 10^9 Pa to 4.0939 x 10^9 Pa and 4.6412 x 10^7 Pa to 2.2281 x 10^8 Pa respectively. It also provides an intermediate safety factor from 0.26 to 0.87 and an endurance limit from 10^3 to 10^6 for residual runs, which is also not suitable to design the screw shaft [32,36].

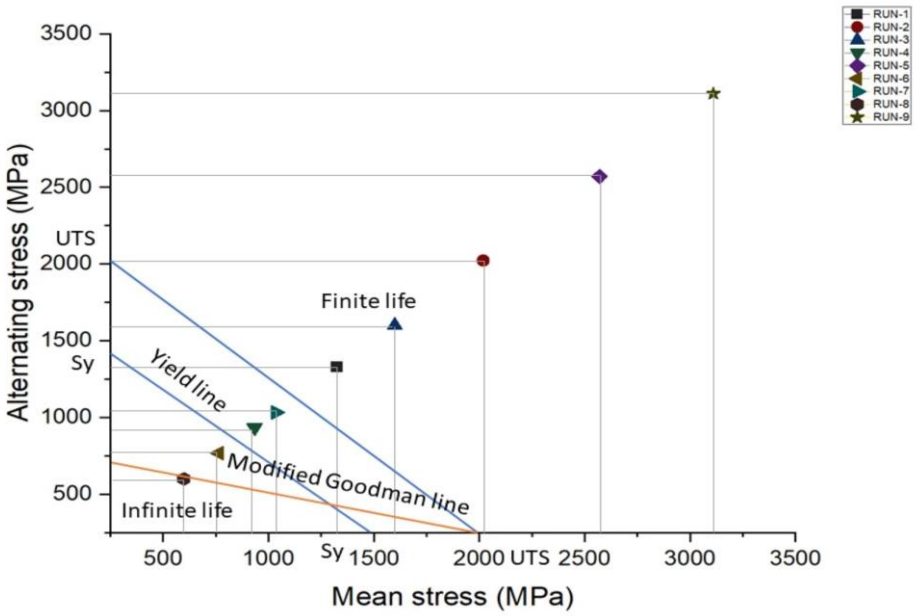

Figure 3. Goodman life diagram for calculating the endurance cycle of the screw shaft.

From the above details, it is noted that the bending and shear stress is gradually increased with decreasing the diameter and increasing the length of the shaft. The safety factor calculated in Table S4 shows a noticeable increase when decreasing the helix angle of the screw. Also, the bendability of the screw is decreased by increasing the helix angle. It is observed that the bending stress decreased as a result of increasing pitch length at the constant diameter of the shaft, which shows that the pitch can indirectly influence the bending and shear stress of the screw shaft. The thread occurs very close for a shorter pitch that can evenly distribute the higher stress over the length of the shaft at a given torque. Hence, run-8 shows a shorter length, larger pitch, diameter, and helix angle which is accepted for designing the safe screw shaft.

Total deformation and its factor of safety experienced by the screw shaft

Fig. S5a,b represents the total deformation and FOS, which was determined for each run of Taguchi's design. In this regard, the maximum deformation of 5.5917 mm was acting on the mid-section of run-2 shown in Fig S5a. Likewise, run-8 shows the minimum deformation of 0.457 mm acting on the mid-section of the screw shaft. In addition, the second and third minimum deformation were experienced by run-6 and 7 which shows the larger diameter and shorter flight length. Run-4, 6, 8, and run-1, 3, and 7 also show that the deformation gives direct proportionality with flight length at a constant diameter. Hence, it is observed that the shaft with a shorter length provides less deformation than the larger flight length.

In Goodman's calculation, the safety factor was calculated using mean bending and shear stress experienced by the shaft. It can endure stress 1.2 times higher than the allowable stress of the material. Now, the principal and shear stress were used for determining the safety factor of the screw shaft. From Fig. S5b, it is observed that the FOS range from 3.94 to 15 was considered a safe design under static and dynamic conditions of the shaft. It shows that the structure can resist the maximum stress of 3.5 to 15

times more than the allowable stress. In specific, the safety factor is comparatively less for runs-1, 2, and 8 due to the minimum helix angle of the screw but these values are not considered inappropriate dimensions for designing the screw shaft. The design with an optimal safety factor suggests the economic structure of the screw shaft for the given hydrothermal process. In the case of FOS, all nine runs are applicable for designing the screw shaft with more reliability and cost-efficient.

Conversion of multiple responses to single response using GRG optimization

The numerical results of each response variable obtained from transient structural simulation are given in Table S5. The multiple responses like principal stress, shear stress, bending stress, bending moment, and total deformation were converted to a single response, called GRG. Initially, the response parameters were converted into normalized values. Then, the computed deviation can be applied to find the GRC values using Eq. (12) for individual runs. Further, Table S6 provides the values of grey relational grade determined by taking the mean of GRC values of respective runs [20]. Finally, the rank was allocated to each run depending on the highest to lowest GRG values given in Table S6. From the GRG analysis, it is observed that run-8 is positioned as rank-1 due to the higher GRG value of 0.992 and run-9 acquired the GRG value of 0.434, positioned as rank-9. It suggested that the dimensions of run-8 are preferred to design the screw shaft.

The Grey Fuzzy Reasoning Grade (GFRG) was predicted to verify the formulated GRG values. In this regard, the Mamdani interface system was applied to relate the input factors like flight length, pitch, helix angle, and depth and also consider the GRG value as output. The linguistic variable was assigned to each level of input parameters as low, medium, and high shown in Fig. S6a. Likewise, it was specified to output parameters as extremely low, very low, low, low medium, medium, high, very high, and extremely high as expressed in Fig. S6b of a certain range from 0.434 to 0.992 as given in Table S7. Then, these linguistic variables were assisted in formulating the nine fuzzy rules based on certain conditions as given in Table S8. Moreover, Fig. S7. illustrates the fuzzy interface system that provides the values of GFRG depending on customized fuzzy rules. It shows the GFRG value of run-8, which is the higher value among other runs. It also provides the intermediate responses to their corresponding inputs, which helps to understand the variation of GFRG value.

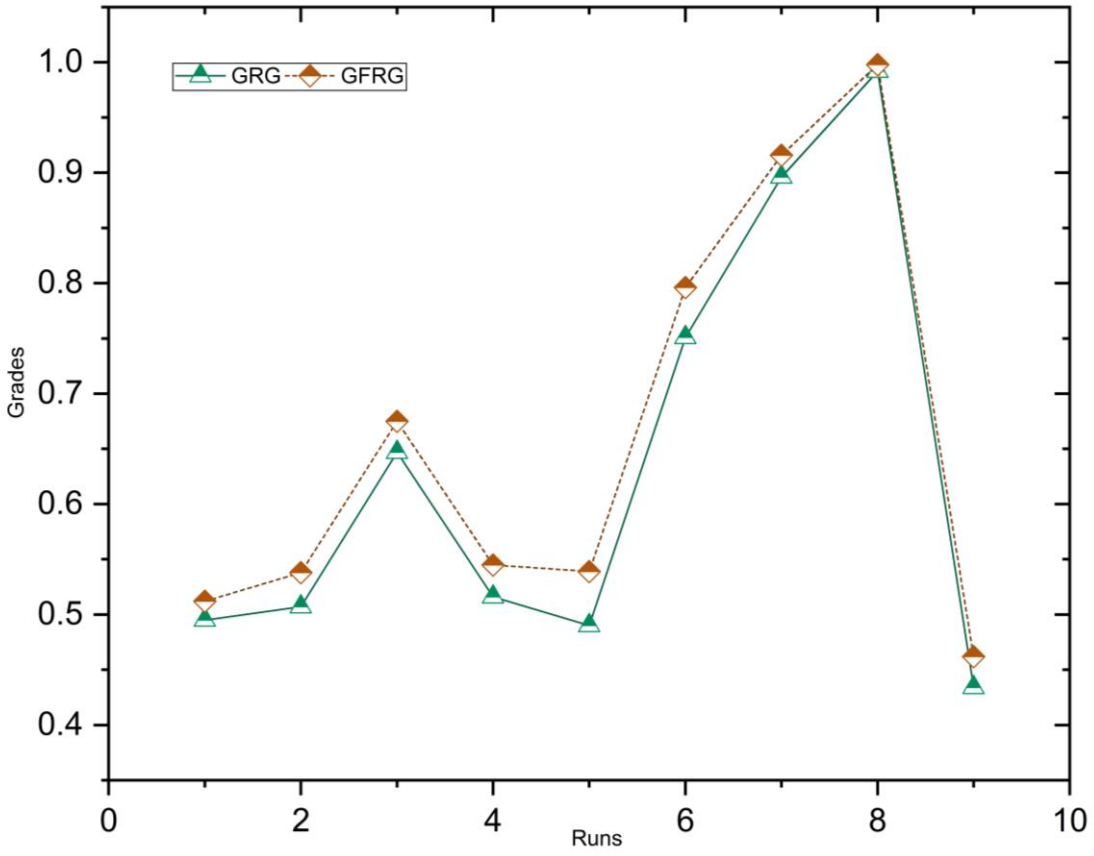

Figure 4. Comparison of grades concerning simulation trials.

The behavior of the response parameters in terms of GRG and GFRG values are given in Table S9 and the graphical representation is shown in Fig. 4. Whence, it is observed that the GFRG is improved up to 6.1 % as compared to GRG, which implies the reduction of fuzziness in the simulation system. Aforementioned in the previous section, run-8 shows the higher GFRG value of 0.998 and is positioned as rank-1 as given in Table S9 and Fig. 4, and is preferred to design the screw shaft.

Signal-to-Noise analysis using GFRG

Signal-to-Noise analysis given in Table S10 provides the ranking method to select the prominent control factors based on the delta value, which is the deviation between the actual and target value of the response variable, GFRG. Higher and lower delta values suggested the extreme and moderate deviation of the response with respect to the control factors. In this regard, the depth of the screw shaft possesses a higher delta value of 3.272 and is positioned as rank-1. Likewise, flight length and pitch show intermediate deviations of 2.52 and 1.25 ranked as 2 and 3 respectively. The Helix angle shows the minimum delta value of 0.76 and is positioned as rank-4, which shows the less significant factor for a corresponding response. These values were compared with the SN ratio graph shown in Fig. 5b, which also suggests the similar behavior of the control factors concerning GFRG. From Fig. 5b, it is observed that flight length and depth showed a higher deviation from the mean than other factors as mentioned in Table S11. Moreover, Fig. 5 also preferred the shorter flight length and depth of 1160 mm and 7.25 mm, nominal pitch, and helix angle of 21.75 mm and 6.8° respectively for reducing the direct responses acting on the screw shaft.

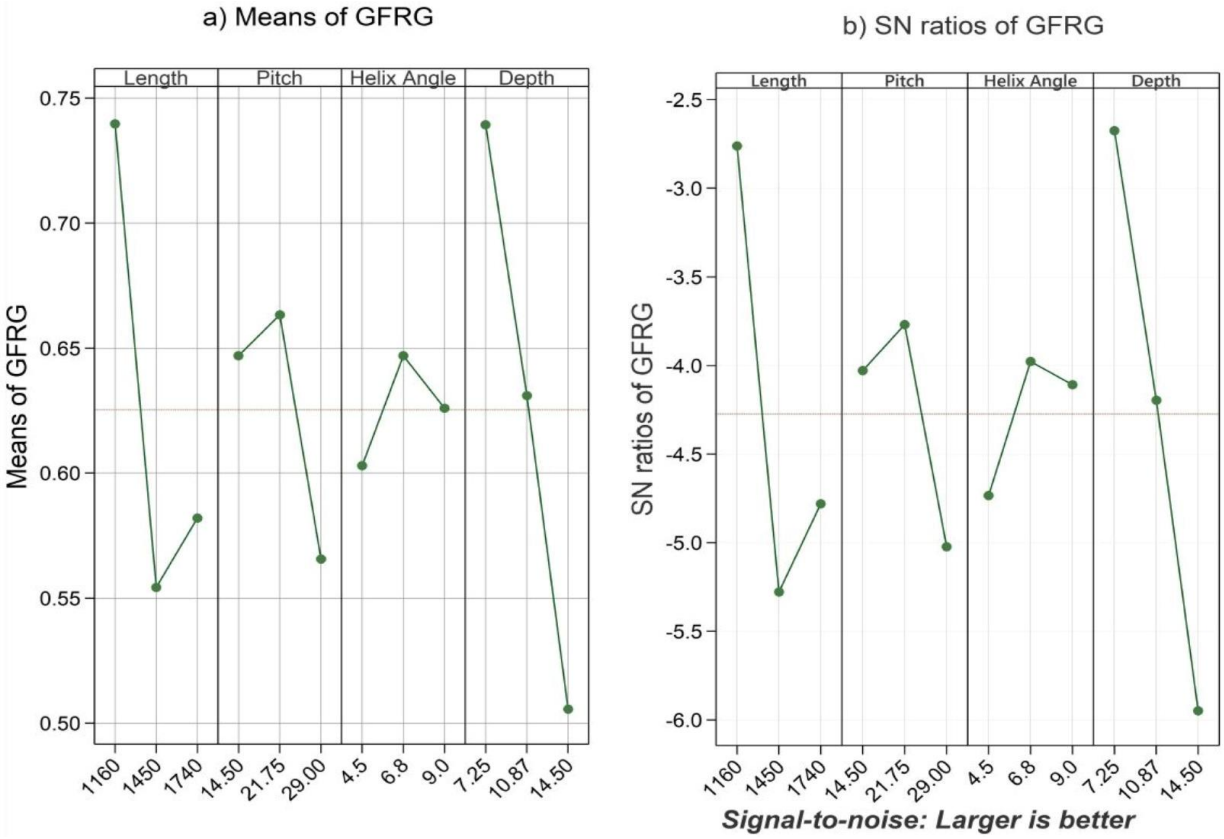

Figure 5. Means and SN ratios of grey fuzzy relational grade.

Single response optimization using GFRG

ANOVA was employed to calculate the contribution of each dimensional factor with respect to a single response referred to as GFRG. It suggests that flight length is the most significant factor with a contribution of 31.52%. Likewise, pitch, helix angle, and depth also convey the noticeable contributions of 27.96%, 22.5%, and 18.02%. The *P*-values calculated in Table S11 were less than 0.05 which rejects the null hypothesis with the acceptance of the alternative hypothesis. It shows potential intent toward the deviation of the GFRG from the mean value. Moreover, Table S11 provides the estimated *R*-squared and adjusted *R*-squared values as 99.34% and 97.36% which also shows the vital deviation in the GFRG with respect to different levels of dimensional factors. Nevertheless, flight length, pitch, helix angle, and depth were crucial factors for controlling direct responses like

principal stress, shear stress, bending stress, bending moment, and total deformation. Eq. (16) proposed the regression equation to find the intermediate GFRG with respect to input factors.

The regression equation for calculating the intermediate GFRG value is given by:

$$GFRG = 0.6700 + 0.1537\ w_1 - 0.0510 w_2 - 0.1027 w_3 + 0.0637 x_1 + 0.0547\ x_2 - 0.1183 x_3 + 0.8231 y_1 + 0.0463\ y_2 - 0.01083\ y_3 + 0.1093\ z_1 + 0.0310\ z_2 - 0.1403 z_3 \quad (16)$$

where, w - flight length, x - pitch, y - helix angle and z - depth.

Confirmation test for the screw shaft

When analyzing the various results obtained from both numerical and statistical methods for the given response variable, it is capable of determining the optimum dimensions for designing the efficient screw shaft. Initially, the two sets of dimensions were selected as 1160 mm, 14.5 mm, 4.5°, 7.25 mm, and 1160 mm, 14.5 mm, 9°, and 7.25 mm based on the results of GFRG and SN analysis. The final transient structural analysis was performed to get the perfect set of values from the above-mentioned dimensions. Fig. 6a,b reveals that similar values of bending stress and bending moment were obtained for both analyses. The values of principal and shear stress possess 9.8% and 37.5% higher internal resistance in SN analysis when compared to GFRG analysis. In the case of total deformation, the value acquired from SN analysis shows 87.5% less deformation compared to GFRG analysis. Even though slight increment in principal and shear stress, this highest value is limited within the ultimate stress of H13. In addition, the total deformation is the most considerable response to design the screw shaft among other responses. Hence, the optimized dimensions obtained from the SN analysis were preferred to design the screw shaft. The optimum values of flight length, pitch, helix angle, and depth were selected as 1160 mm, 21.75 mm, 6.8°, and 7.25 mm respectively.

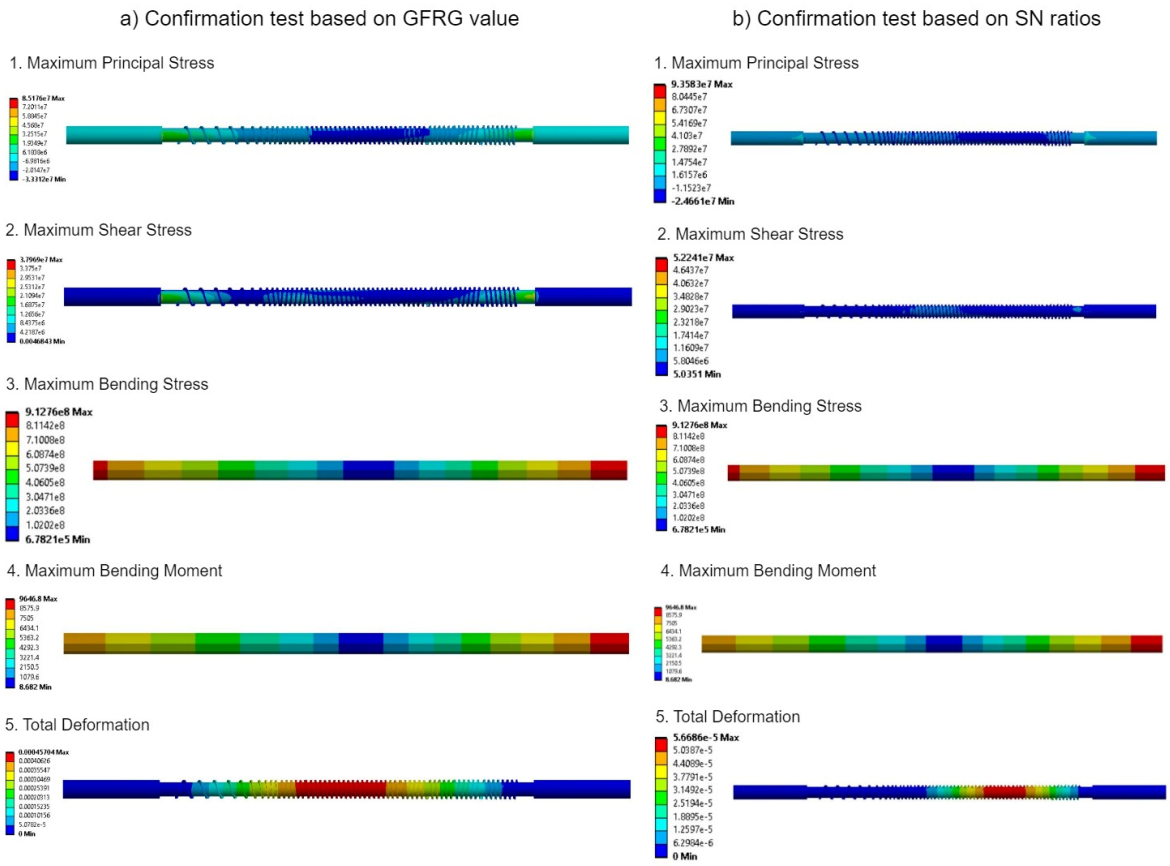

Figure 6. Confirmation structural analysis depends on GFRG and SN analysis.

CONCLUSION

The optimal screw shaft has been designed for the high-pressure HTCL reactor with the help of FEM followed by statistical optimization using GRG, GFRG, ANOVA, and Taguchi's method. Maximum principal stress, maximum shear stress, maximum bending

stress, total bending moment, and deformation were taken as the crucial response variables for dimensional optimization of depth, helix angle, flight, and pitch length. It is observed that the dimensional parameters present in run-8 show the minimum stress and total deformation. In addition, the Goodman method also conveys that run-8 has ensured a higher safety limit and endurance limit of 1.20 and 10^7 cycles respectively. The above-mentioned five response variables were successfully converted into a single response termed GRG during multi-response optimization. The result possesses that run-8 dimensions have the highest GRG and GFRG value of 0.992 and 0.998 respectively, and it is suitable for designing the screw shaft. Conversely, the SN ratio from Taguchi analysis suggests a slightly modified dimension in helix angle compared to run-8. The two sets of dimensions were taken for confirmation test as set-1 consists of flight length=1160 mm, depth=7.25 mm, helix angle=4.5°, pitch length=14.5 mm, and set-2 comprise of flight length=1160 mm, depth=7.25 mm, helix angle=6.8°, and pitch length=21.75 mm depending on the results from GFRG and SN analysis respectively. From the confirmation results, it is recommended that the dimensions obtained from the SN analysis provide very little deformation of 0.0566 mm, which is 87.5 % lower than the deformation formed in the dimensions of the GFRG analysis. From the above details, the optimal dimensions were selected from SN analysis (set-2) as 1160 mm, 14.5 mm, 9°, and 7.25 mm for respective flight length, pitch, helix angle, and depth of the screw shaft.

ACKNOWLEDGMENTS

This research work was supported by the Department of Science and Technology, Ministry of India under the sanction order no. DST/TDT/WMT/Plastic Waste/2021/08(G)&(C). This research article is based on numerical simulations and optimization conducted by the authors. The authors would like to thank all the researchers who contributed to the research work. Throughout this study, the authors acknowledge Kongu Engineering College for their support of the research facility.

REFERENCES

[1] C.D. Venkatachalam, S.R. Ravichandran, M. Sengottian, Environ. Eng. Res. 27(2021), 200555-200571. https://doi.org/10.4491/eer.2020.555.

[2] F. Campuzano, R.C. Brown, J.D. Martínez, Renew. Sust. Energ. Rev. 102(2019), 372-409. https://doi.org/10.1016/j.rser.2018.12.014.

[3] S.S. Toor, L.A. Rosendahl, A. Rudolf, Energy 36 (2011), 2328-2342. https://doi.org/10.1016/j.energy.2011.03.013.

[4] C.D. Venkatachalam, M. Sengottian, S.R. Ravichandran, K. Subramaniyan, P. Kalappan Thangamuthu, Period. Polytech. Chem. Eng. 65 (2020), 105-115. https://doi.org/10.3311/PPch.15187.

[5] M.S. Wahyudiono, M. Goto, Fuel 88 (2009) 1656-1664. https://doi.org/10.1016/j.fuel.2009.02.028.

[6] B. Miljkovic, Period. Polytech. Chem. Eng. 67 (2023) 62-73. https://doi.org/10.3311/PPch.20257.

[7] M.S. Wahyudiono, M. Goto, Chem. Eng. Process 47 (2008) 1609-1619. https://doi.org/10.1016/j.cep.2007.09.001.

[8] I.M. Sintamarean, I.F. Grigoras, C.U. Jensen, S.S. Toor, T.H. Pedersen, L.A. Rosendahl, Biomass Convers. Biorefin. 7 (2017) 425-435. https://doi.org/10.1007/s13399-017-0247-9.

[9] P. Brassard, S. Godbout, V. Raghavan, J.H. Palacios, M. Grenier, D. Zegan, Energies 10 (2017) 288-302. https://doi.org/10.3390/en10030288.

[10] G. Shengbo, Y. Peter Nai Yuh, C. Yoke Wang, X. Changlei, W.M. Wan Adibah, L. Rock Keey, P. Wanxi, Y. Tong-Qi, T. Meisam, A. Mortaza, S.k. Christian, L. Su Shiung, Renew. Sust. Energ. Rev. 135(2021) 110148-110162. https://doi.org/10.1016/j.rser.2020.110148.

[11] C.E. Efika, C. Wu, P.T. Williams, J. Anal. Appl. Pyrolysis 95(2012) 87-94. https://doi.org/10.1016/j.jaap.2012.01.010.

[12] S.K. Hoekman, A. Broch, L. Felix, W.E. Farthing, Energy Convers. Manag. 134(2017) 247-259. https://doi.org/10.1016/j.enconman.2016.12.035.

[13] P. Evangelopoulos, H. Persson, E.K. Kantarelis, W. Yang, Process Saf. Environ. Prot. 143 (2020) 313-321. https://doi.org/10.1016/j.psep.2020.07.006.

[14] S. Ge, P.N.Y. Yek, Y.W. Cheng, C. Xia, W.A.W. Mahari, R.K. Liew, P. Wanxi, Y. Tong-Qi, T. Meisam, A. Mortaza, S.k. Christian, L. Su Shiung, Renew. Sust. Energ. Rev. 135 (2021) 110148-110162. https://doi.org/10.1016/j.rser.2020.110148.

[15] L. Halasz, Period. Polytech. Chem. Eng. 34 (1989) 173-196. https://pp.bme.hu/ch/article/view/2721.

[16] A.Y. Doost, D.L. William, Sustainability 12 (2020) 7352-7385. https://doi.org/10.3390/su12187352.

[17] M. Meise, L. Jäger, A. Wilk, T. Heitmann, S. Scholl, Chem. Ing. Tech. 92 (2020) 1074-1082. https://doi.org/10.1002/cite.202000092.

[18] E.P. Bilalis, M.S. Keramidis, N.G. Tsouvalis, Mar. Struct. 84 (2022) 103194. https://doi.org/10.1016/j.marstruc.2022.103194.

[19] S.P.S. Kumar, R. Rao, B.A. Rajeevalochanam, Procedia Eng. 55 (2013) 499-509. https://doi.org/10.1016/j.proeng.2013.03.287.

[20] C. Moganapriya, R. Rajasekar, P. Sathish Kumar, T. Mohanraj, V.K. Gobinath, J. Saravanakumar, Struct. Multidiscip. Optim. 63 (2020) 1169-1186. https://doi.org/10.1007/s00158-020-02751-9.

[21] S. Ajith Arul Daniel, R. Pugazhenthi, R. Kumar, S. Vijayananth, Def. Technol. 15 (2019) 545-556. https://doi.org/10.1016/j.dt.2019.01.001.

[22] S.M. Senthil, R. Parameshwaran, S. Ragu Nathan, M. Bhuvanesh Kumar, K. Deepandurai, Struct. Multidiscipl. Optim. 62 (2020) 1117-1133. https://doi.org/10.1007/s00158-020-02542-2.

[23] F. Xiong, D. Wang, S. Zhang, K. Cai, S. Wang, F. Lu, Struct. Multidiscipl. Optim. 57 (2017) 441-461. https://doi.org/10.1007/s00158-017-1749-6.

[24] W. Yao, K. Cai, Y. Xu, Optimizing the beam-like structure of a vehicle body using the grey-fuzzy-Taguchi method 53 (2020) 49-70. https://doi.org/10.1080/0305215X.2019.1698033.

[25] M. Saleh, Z. Zaidi, M.H. Ionescu, C. Hurt, K. Short, J.E. Daniels, P. Munroe, L.E. Edwards, D. Bhattacharyya, Int. J. Plast. 86 (2016) 151-169. https://doi.org/10.1016/j.ijplas.2016.08.006.

[26] V.A. Girisha, M.M. Joshi, L.J. Kirthan, A. Bharatish, R. Hegde, Sādhanā 44 (2019) 1-8. https://doi.org/10.1007/s12046-019-1111-3.

[27] H. Kweon, J. Kim, O. Song, D. Oh, Nucl. Eng. Technol. 53 (2021) 647-656. https://doi.org/10.1016/j.net.2020.07.014.

[28] B. Bozorgmehri, V.-V. Hurskainen, M. K. Matikainen, A. Mikkola, J. Sound Vib. 453 (2019) 214-236. https://doi.org/10.1016/j.jsv.2019.03.022.

[29] R. Scheepers, P.S. Heyns, J. Mech. Sci. Technol. 30 (2016) 4063-4074. https://doi.org/10.1007/s12206-016-0819-9.

[30] N.L. Pedersen, J. Strain Anal. Eng. 56 (2020) 195-205. https://doi.org/10.1177/0309324720969530.

[31] O.A. Samuel, I.O. Bankole, O.I. Christianah, O.M.A. Adeyinka, F.K. Joseph, J. Mater. Res. 8 (2019) 105-111. https://doi.org/10.1016/j.jmrt.2017.10.007.

[32] Á. Sass, A. Kummer, Z. Ulbert, A. Egedy, Period. Polytech. Chem. Eng. 65 (2021) 536-549. https://doi.org/10.3311/PPch.17095.

[33] Z. Yongjie No, X. Hongmei No, Appl. Eng. Agric. 35 (2019) 453-460. https://https://doi.org/10.13031/aea.13351.

[34] S. Seifoori, A. Mahdian Parrany, M. Khodayari, Eng. Fail. Anal. 116 (2020) 104752-104768. https://doi.org/10.1016/j.engfailanal.2020.104752.

[35] L. Dao-Kui, L. Xian-Fang, Cr Mecanique 344 (2016) 556-568. https://doi.org/10.1016/j.crme.2016.01.007.

[36] A. Roy, P. Palit, S. Das, G. Mukhyopadyay, Eng. Fail. Anal. 112 (2020) 104511-104526. https://doi.org/10.1016/j.engfailanal.2020.104511.

[37] K. Cai, D. Wang, Struct. Multidiscipl. Optim. 56 (2017) 1539-1553. https://doi.org/10.1007/s00158-017-1728-y.

[38] Q. Sawei, X. Zhigang, H. Hong, Y. Zhong, X. Erli, X. Congchang, L. Luoxing, Struct. Multidiscipl. Optim. 64 (2021) 4129-4145. https://doi.org/10.1007/s00158-021-03035-6.

[39] A. Tanmaya, G. Raghvendra, A. Sudeekcha, S. Vishal, K. Manish, K. Saket, Sustain. Futures 2 (2020) 100039-100050. https://doi.org/10.1016/j.sftr.2020.100039.

[40] X. Deng, S. Wang, H. Youssef, L. Qian, Y. Liu, Struct. Multidiscipl. Optim. 62 (2020) 2833-2847. https://doi.org/10.1007/s00158-020-02640-1.

[41] D. Sunil, R.N. Suresh Kumar, Measurement 169 (2021) 108340-108347. https://doi.org/10.1016/j.measurement.2020.108340.

[42] B. Maël, B. Johan, V. Laura, R.-C. Ainhoa, C. Edwin, Renew. Energy. 172 (2021) 941-954. https://doi.org/10.1016/j.renene.2021.03.076.

[43] M.A. Perras, H. Wannenmacher, M.S. Diederichs, Rock Mech. Rock Eng. 48 (2014) 1647-1671. https://doi.org/10.1007/s00603-014-0656-z.

[44] W. Zhang, J. Yang, C. Li, R. Dai, A. Yang, J. Vib. Control 23 (2016) 1183-1192. https://doi.org/10.1177/1077546315590908.

CHITRA DEVI VENKATACHALAM[1]

PREMKUMAR BHUVANESHWARAN[1]

MOTHIL SENGOTTIAN[2]

SATHISH RAAM RAVICHANDRAN[2]

[1]Department of Food Technology, Kongu Engineering College, Perundurai, Tamil Nadu, India.

[2]Department of Chemical Engineering, Kongu Engineering College, Perundurai, Tamil Nadu, India

NAUČNI RAD

PROJEKTOVANJE ZASNOVANA NA POUZDANOSTI OPTIMIZACIJA PUŽNE OSOVINE ZA KONTINUALNI PROCES HIDROTERMALNE KO-LIKVEFAKCIJE VISOKOG PRITISKA

Hidrotermalna ko-likvefakcija (HTKL) je istaknuti proces za proizvodnju bioproizvoda sa većom brzinom konverzije. Izvodi se na visokim temperaturama i pritisku u prisustvu vode. Ranije se uglavnom sprovodio u šaržnim reaktorima, koji imaju velika ograničenja uključujući radnu zapreminu, povratno mešanje i tegoban proces za visoku produktivnost. S tim u vezi, ovo istraživanje je sprovedeno s ciljem projektovanja pužne osovine za HTKL proces visokog pritiska. Dimenzionalni faktori, uključujući dužinu kretanja, korak, ugao spirale i dubinu, uzeti su u obzir da bi se dizajnirala optimalna pužna osovina. Isto tako, glavni naponi, napon smicanja, napon savijanja, moment savijanja i ukupna deformacija smatrani su neizbežnim odzivnim promenljivima za analizu unutrašnje čvrstoće osovine. U tom smislu, Taguči L9 (34) ortogonalni niz je korišćen kao eksperimentalni plan. Zatim su numerički rezultati analize prelazne strukture analizirani uz pomoć statističkih metoda kako bi se pronašle najuticajnije dimenzije za minimiziranje odzivnih promenljivih. Shodno tome, upoređeni su rezultati različitih metoda i izabrani su najoptimalniji parametri.

Ključne reči: hidrotermalna ko-likvefakcija, pužna osovina, metoda konačnih elemenata, analiza napona, Gudmanovi kriterijumi otkaza, tehnika optimizacije višestrukog i jednog odziva.